Neuron
Article

Conditions and Constraints for Astrocyte Calcium Signaling in the Hippocampal Mossy Fiber Pathway

Martin D. Haustein,[1] Sebastian Kracun,[1] Xiao-Hong Lu,[3] Tiffany Shih,[4] Olan Jackson-Weaver,[1] Xiaoping Tong,[1] Ji Xu,[1] X. William Yang,[3] Thomas J. O'Dell,[1] Jonathan S. Marvin,[5] Mark H. Ellisman,[4] Eric A. Bushong,[4] Loren L. Looger,[5] and Baljit S. Khakh[1,2,*]
[1]Department of Physiology
[2]Department of Neurobiology
[3]Center for Neurobehavioral Genetics, Semel Institute for Neuroscience and Human Behavior
David Geffen School of Medicine, University of California Los Angeles, Los Angeles, CA 90095-1751, USA
[4]National Center for Microscopy and Imaging Research and Department of Neurosciences, University of California San Diego, La Jolla, CA 92093, USA
[5]Janelia Farm Research Campus, Howard Hughes Medical Institute, Ashburn, VA 20147, USA
*Correspondence: bkhakh@mednet.ucla.edu
http://dx.doi.org/10.1016/j.neuron.2014.02.041

SUMMARY

The spatiotemporal activities of astrocyte Ca^{2+} signaling in mature neuronal circuits remain unclear. We used genetically encoded Ca^{2+} and glutamate indicators as well as pharmacogenetic and electrical control of neurotransmitter release to explore astrocyte activity in the hippocampal mossy fiber pathway. Our data revealed numerous localized, spontaneous Ca^{2+} signals in astrocyte branches and territories, but these were not driven by neuronal activity or glutamate. Moreover, evoked astrocyte Ca^{2+} signaling changed linearly with the number of mossy fiber action potentials. Under these settings, astrocyte responses were global, suppressed by neurotransmitter clearance, and mediated by glutamate and GABA. Thus, astrocyte engagement in the fully developed mossy fiber pathway was slow and territorial, contrary to that frequently proposed for astrocytes within microcircuits. We show that astrocyte Ca^{2+} signaling functionally segregates large volumes of neuropil and that these transients are not suited for responding to, or regulating, single synapses in the mossy fiber pathway.

INTRODUCTION

Important progress has been made in understanding the roles of glia in the brain since their discovery over a century ago and following landmark physiological studies (Kuffler, 1967). Astrocytes (a subclass of glia) are known to display dynamic intracellular Ca^{2+} signals (Agulhon et al., 2008; Li et al., 2013), and it has recently been shown that astrocytes rapidly sense and regulate single synapses (Di Castro et al., 2011; Panatier et al., 2011). In these settings, astrocytes respond to single synapse glutamate release by exhibiting localized intracellular Ca^{2+} elevations in their main processes a few micrometers from the soma, implying that they are actively involved in microcircuit function (Di Castro et al., 2011; Panatier et al., 2011). However, abolishing one major form of intracellular Ca^{2+} signal within astrocytes was without obvious consequence for neuronal function (Agulhon et al., 2010; Fiacco et al., 2007; Petravicz et al., 2008). To understand these differences, one needs to explore when astrocytes become excited within neuronal circuits, but this has proven challenging. Unlike neurons, astrocytes are not electrically excitable and evaluations have had to rely on imaging. In particular, available imaging methods that use organic Ca^{2+} indicator dyes are not ideal for monitoring astrocyte branches, which are the primary sites for interactions with neurons (Reeves et al., 2011; Shigetomi et al., 2010, 2013a; Tong et al., 2013). As a result, the function of astrocyte Ca^{2+} signaling within neuronal circuits remains incompletely explored (Tong et al., 2013).

We have refined optical and genetic tools in order to study astrocyte branches and territories by building on recent progress with genetically encoded calcium indicators (GECIs) (Tian et al., 2012). GECIs are not a panacea, and they have effects such as Ca^{2+} buffering that are shared with organic dyes. However, under most circumstances they do not obviously perturb neurons or astrocytes and are complementary to other approaches (Chen et al., 2013; Shigetomi et al., 2013a, 2013b; Tian et al., 2009; Zariwala et al., 2012).

To image cytosolic and near-membrane Ca^{2+}, we used astrocyte-specific expression of cytosolic GCaMP3 or membrane-targeted Lck-GCaMP3, respectively (Shigetomi et al., 2010, 2011, 2013a; Tian et al., 2009). To directly image astrocyte cell-surface glutamate signals, we used a genetically encoded glutamate sensor (Marvin et al., 2013) (iGluSnFR). We also used GCaMP6f, a recent GECI with kinetics similar to the organic Ca^{2+} indicator dye OGB1-AM (Chen et al., 2013). In order to drive neurotransmitter release selectively from the mossy fiber pathway, we generated novel BAC transgenic "*SPRAE*" mice that express a drug-activated ion channel within the mossy fiber pathway. Using these optical and pharmacogenetic tools, we explored astrocyte signaling in the circuit formed by the dentate gyrus granule cell projection (the mossy fiber pathway) to the

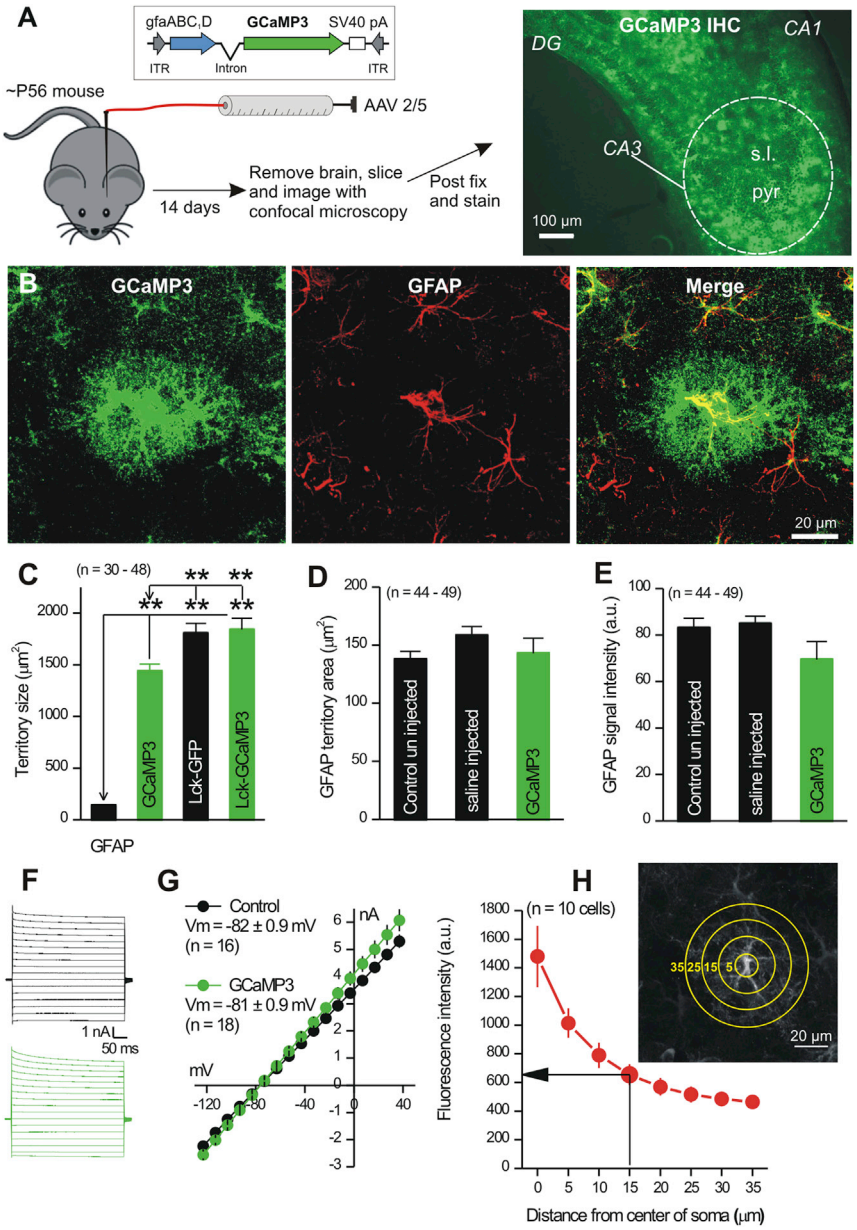

Figure 1. Expression of GCaMP3 in Astrocytes

(A) The cartoon illustrates the procedure to inject AAV2/5 capable of expressing GCaMP3 in s.l. astrocytes of P56 mice. The right hand image shows fluorescence signal for GCaMP3 detected by immunohisochemistry (IHC) in the CA3 region (DG indicates dentate gyrus; pyr indicates pyramidal cell layer).

(B) GCaMP3 and GFAP expression in an astrocyte from the s.l. region. The GCaMP3-expressing astrocyte was GFAP positive and 85% ± 2% of all GFAP-positive astrocytes in the s.l. expressed GCaMP3 (n = 4 mice).

(C) Maximal projection territory area for GFAP, GCaMP3, Lck-GCaMP3, and Lck-GFP.

(D and E) GFAP maximal projection territory area (D) and intensity (E) for astrocytes.

(F and G) Traces and average data for astrocyte current-voltage relationships (−120 to +40 mV) from control mice or those microinjected with GCaMP3.

(H) The image shows a representative astrocyte with circles drawn radially (5 µm spacing). Such circles were used to measure the intensity of GCaMP3 expression at increasing distances from the center of the soma (in the graph). The highest intensity was in the soma, which has the largest volume, and intensity fell with distance. Average data are shown as mean ±SEM.

CA3 region of the hippocampus (Amaral and Lavenex, 2007). We chose this circuit because mossy fibers are the only feed-forward excitatory input to the anatomically well-defined CA3 region of the stratum lucidum (s.l.) (Amaral and Lavenex, 2007; Ruiz and Kullmann, 2012; Spruston and McBain, 2007). Additionally, the anatomical relationship between mossy fibers and postsynaptic neuronal and astrocytic targets has been described by electron microscopy (Rollenhagen and Lübke, 2006; Rollenhagen et al., 2007; Wilke et al., 2013).

RESULTS

We deployed several imaging tools to study astrocytes located in the s.l. of the adult mouse hippocampus (~P70). The slices were ~300 µm thick, and the imaged astrocytes were located ~40 µm from the slice surface. The experiments were conducted at room temperature (~21°C) or close to mouse body temperature (34°C), as indicated. The imaging was performed using laser scanning confocal microscopy with a 40× objective lens with a numerical aperture of 0.8. The effective pixel size was 0.2 × 0.2 µm, which is larger than the size of astrocyte branchlets at <100 nm.

GCaMP3 Reveals Stratum Lucidum Astrocyte Branches and Territories

We could not reliably load hippocampal astrocytes from adult mice with organic Ca^{2+} indicator dyes. By extending tool development work that showed GCaMP3 is well suited to study astrocytes from adult mice (Shigetomi et al., 2013a, 2013b), we used it, Lck-GCaMP3, and GCaMP6f to explore s.l. astrocyte intracellular Ca^{2+} signals. For selective expression within astrocytes, we used adeno-associated viruses of the 2/5 serotype (AAV 2/5) and the astrocyte-specific *gfaABC$_1$D* promoter (Shigetomi et al., 2013a) (Figure 1). GECIs were innocuously expressed within large parts of s.l. astrocyte territories, including their branches. Furthermore, AAV2/5-mediated expression of fluorescent proteins does not alter spontaneous Ca^{2+} signals in astrocytes (Shigetomi et al., 2013a), which recalls and extends past work with neurons that reported little deleterious effect of GECI expression (Chen et al., 2013; Shigetomi et al., 2013b; Tian et al., 2009; Zariwala

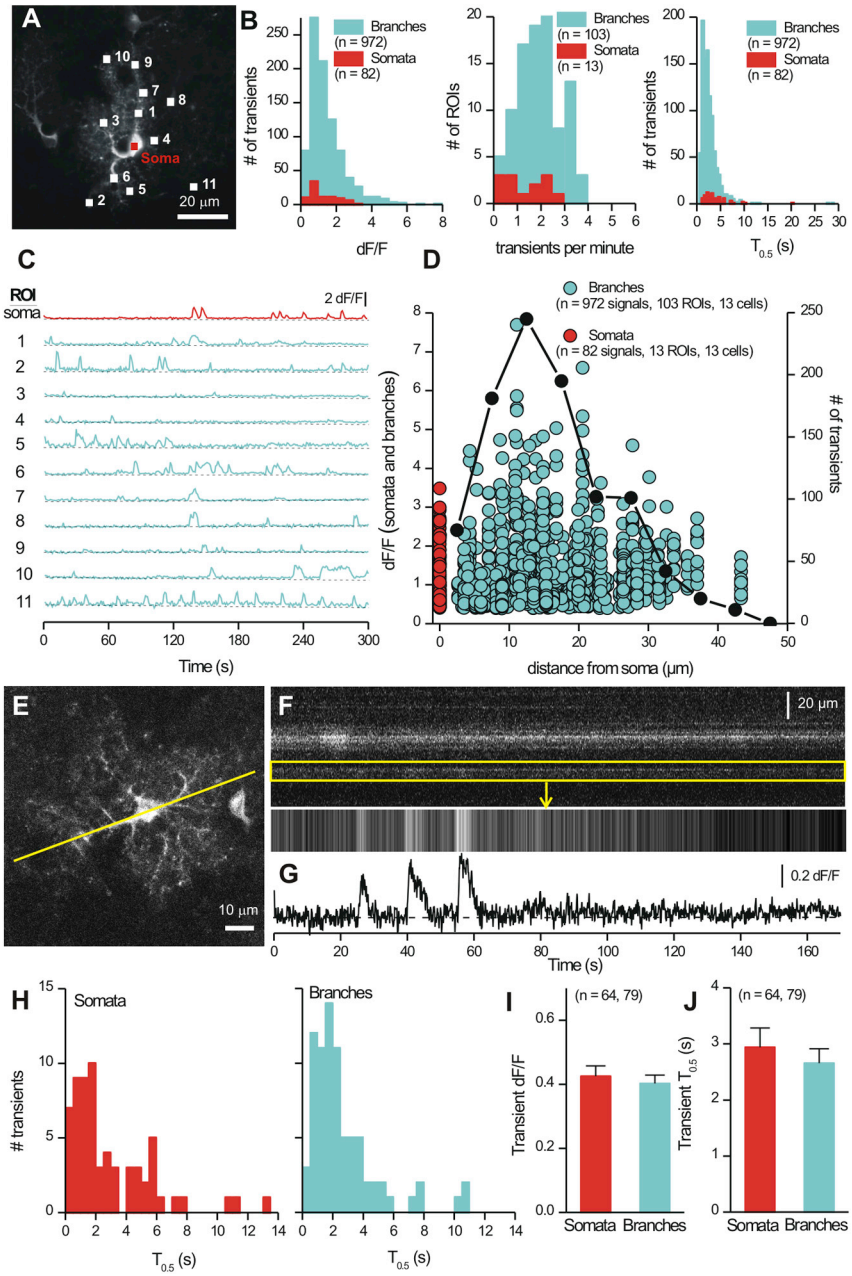

Figure 2. Properties of Ca^{2+} Signals in s.l. Astrocytes

(A) Image of a single s.l. astrocyte expressing GCaMP3 with 11 ROIs indicated (Movie S1).

(B) Distributions of astrocyte Ca^{2+} signal properties (blue bars are for branches, and the red bars are for somata).

(C) Traces for 11 ROIs from Figure 2A.

(D) Plots of Ca^{2+} signal amplitude (left axis) and number (right axis) as a function of distance from the soma. The number of Ca^{2+} signals in 5 μm bins is shown by the black line.

(E) Image of an s.l. astrocyte with a yellow line indicating the approximate position of the region chosen for 200 Hz line scan imaging.

(F) Image of line scan data for the line shown in (E), with an expanded region corresponding to a branchlet shown below. In these images, the x axis is time, and the y axis is distance along the scanned line.

(G) The trace for the selected region shown in (F).

(H) Distributions showing Ca^{2+} signal half-widths from line scan experiments for somatic and branchlet regions.

(I–J) Bar graphs summarize Ca^{2+} signal properties such as dF/F and half-width for line scan data. Average data are shown as mean ±SEM.

et al., 2012). All of the GECIs we used display Ca^{2+} affinities (~0.3 μM) similar to organic dyes often used to study astrocytes.

Stratum Lucidum Astrocytes Display Slow Ca^{2+} Signals that Last Seconds

High numbers of Ca^{2+} signals were observed within s.l. astrocytes expressing GCaMP3 (Movie S1 available online; Figures 2B–2D) (n = 13 astrocytes). Eleven ROIs from an astrocyte are shown in Figures 2A and 2C, illustrating that the soma was relatively silent and that numerous Ca^{2+} signals occurred in branches. Ca^{2+} signals in the somata and branches displayed similar amplitudes and second's time scale kinetics (Figure 2B; Table S1). However, ~8-fold greater numbers of Ca^{2+} signals were measured within branches than in somata (Figure 2B). Such Ca^{2+} signals originated from, and were of similar amplitude within, entire territories of single astrocytes (Figure 2D; n = 13 cells). The greatest numbers were detected ~15 μm from the soma (Figure 2D), perhaps reflecting a region of high astrocyte branching or a larger cytosolic volume per branch at this region. These possibilities cannot be discriminated by light microscopy, and further detailed work employing correlated light and electron microscopy is needed. However, the observed result is not due to fortuitous accumulation of GCaMP3 at ~15 μm (Figure 1H; n = 10 cells).

To determine if fast Ca^{2+} signals existed in s.l. astrocytes, we used 200 Hz line scan imaging (Figure 2E; n = 10). A representative line scan lasting ~170 s is shown in Figure 2F, and a branch region is expanded and plotted as a trace (Figure 2G). Ca^{2+} signals were clearly seen; we repeated the analyses for ten astrocytes and measured transient properties in branches and somata (Figures 2H–2J). These data show that on average the fastest Ca^{2+} signals last ~3 s, which is consistent with the frame scan data (Figures 2B and 2C; Table S1). We also performed a specific set of experiments on single astrocytes to measure astrocyte Ca^{2+} signals at room temperature and then at 34°C. In these pairwise comparisons, we noted

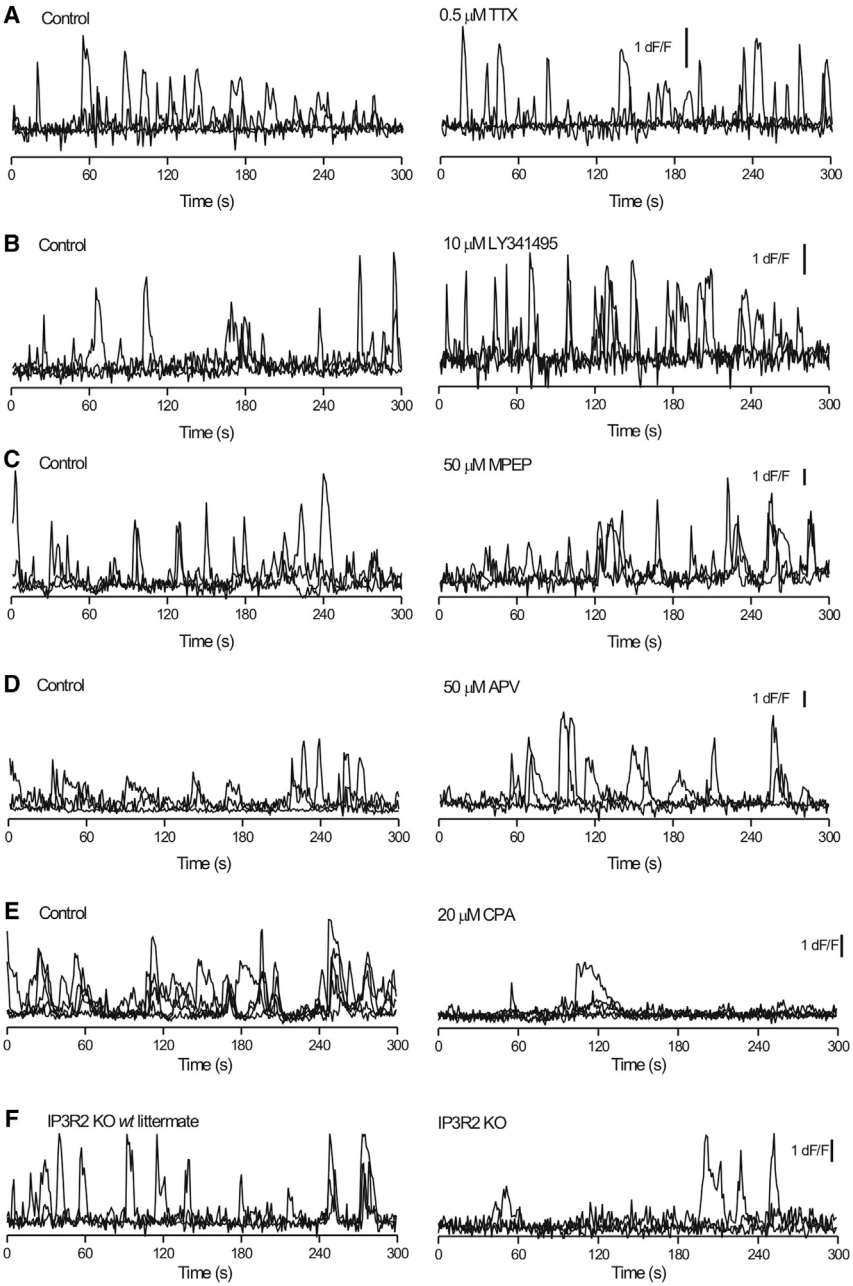

Figure 3. Stratum Lucidum Region Astrocyte Spontaneous Ca^{2+} Signals Are Not Affected when Action Potentials or Glutamate Receptors Are Blocked, but Are Markedly Reduced in Number when Intracellular Ca^{2+} Stores Are Depleted or Disrupted

(A) Four superimposed traces for branchlets under control conditions and then in the presence of 0.5 μM TTX, which had no effect.

(B–D) As in (A), but for experiments when the brain slices were treated with antagonists of mGluR2/3 (10 μM LY341495), mGluR5 (50 μM MPEP), and NMDA receptors (50 μM APV).

(E) As in (A), but for slices treated with cyclopiazonic acid (20 μM CPA) to deplete intracellular Ca^{2+} stores.

(F) Representative traces for spontaneous Ca^{2+} signals recorded from IP3R2 KO mice and their WT littermates. The average data are shown in Figures S1 and S2.

significant changes in the properties of Ca^{2+} signals at warmer temperatures, including acceleration of kinetics in somata, as expected. However, overall the Ca^{2+} signals still lasted seconds (Table S2; n = 7).

Is it possible that fast Ca^{2+} signals were missed with GCaMP3? To address this, we repeated experiments shown in Figure 2 by using GCaMP6f, which displays rapid kinetics and high sensitivity (Chen et al., 2013). GCaMP6f displays larger peak fluorescence changes compared to GCaMP3 (Chen et al., 2013), and in accord, using GCaMP6f astrocyte, spontaneous Ca^{2+} signals were 3-fold larger, and we observed twice as many ROIs with Ca^{2+} signals in the branches (Table S1; n = 14). However, the Ca^{2+} signals detected by GCaMP6f still lasted several seconds (Table S1).

It is conceivable that cytosolic GECIs may miss Ca^{2+} signals in fine processes. To explore this, we used Lck-GCaMP3, which better reports near-membrane Ca^{2+} signals within fine processes (Shigetomi et al., 2013a). However, we found that expression of Lck-GCaMP3 within s.l. astrocytes reported fewer spontaneous Ca^{2+} signals than GCaMP3 (Table S1; n = 12), even though it was expressed within territory areas larger than GCaMP3 (Figure 1C). These data indicate that s.l. astrocytes do not display a significant number of near-membrane Ca^{2+} signals in fine processes. We further explored these possibilities in subsequent experiments, but taken together, these data suggest that s.l. astrocytes are different from stratum radiatum (s.r.) astrocytes (Shigetomi et al., 2013b) in that fewer signals are mediated by near-membrane Ca^{2+} dynamics in the s.l. region. This implies diverse astrocyte properties and functions within subfields of the hippocampus.

Stratum Lucidum Astrocyte Ca^{2+} Signals Are Not Due to mGluRs, NMDARs, or Action Potential Firing

Given the tight association of astrocyte branches and excitatory synapses in the s.l. region (Rollenhagen et al., 2007), we determined if astrocyte Ca^{2+} signals (Figure 2) were driven by release of glutamate, either tonically or that evoked by action potential firing. We found that application of 0.5 μM tetrodotoxin (TTX), to block action potentials, produced no statistically significant change in Ca^{2+} signal dF/F, frequency, or kinetics in somata or branches (Figure 3A; average data in Figures S1A and S1B;

n = 10). Moreover, we found that spontaneous somatic and branch Ca^{2+} signal amplitudes, frequency, and kinetics were not significantly reduced by mGluR5, mGluR2/3, or NMDA receptor antagonists (50 μM MPEP, 10 μM LY341495, and 50 μM APV, respectively) (Figures 3B, 3C, 3D, and S1C–S1H; n = 10 in each case). These reagents also did not markedly change the basal fluorescence of the astrocytes (Figures S1I–S1L). However, depletion of intracellular Ca^{2+} stores with 20 μM cyclopiazonic acid (CPA) for 25 min significantly (>70%) reduced the numbers of Ca^{2+} signals in astrocyte somata and branches, thus pointing to their intracellular origin (Figure 3E; Figures S2A and S2B; n = 5). As expected, CPA significantly elevated the basal fluorescence of astrocytes (Figure S1M). We next used IP3R2 knockout mice (Agulhon et al., 2010; Petravicz et al., 2008) to explore the role of this channel in controlling release of Ca^{2+} from stores. Recalling the CPA data, we found that the IP3R2 KO mice displayed significantly reduced numbers of Ca^{2+} signals compared to wild-type (WT) littermates (by ~60%) (Figure 3F; Figures S2C and S2D; n = 9 cells).

Unexpectedly, the use of GECIs in the IP3R2 KO mice revealed residual Ca^{2+} signals in s.l. astrocyte somata and mainly in branches (Figures S2C and S2D). Thus, although Ca^{2+} signals are reduced in number in the IP3R2 KO mice, they are not abolished when GECIs are deployed to image entire astrocyte territories. Interestingly, the residual Ca^{2+} signals in s.l. astrocytes were not blocked by HC 030031 (Figures S2E and S2F; n = 8), a selective antagonist for TRPA1 channels. In contrast, functional TRPA1 channels are expressed and mediate significant Ca^{2+} signals within s.r. astrocytes (Shigetomi et al., 2013b).

SPRAE Mice Selectively Expressing a Drug-Activated Cation Channel in Mossy Fibers

We considered it important to selectively drive glutamate release from mossy fiber terminals in order to explore astrocyte signaling. As part of an unrelated project (Richler et al., 2008), we created BAC transgenic mice expressing fluorescently tagged P2X2 receptors (P2X2-YC; YC is Yellow Cameleon 3.1) (Figures S3A–S3C) within mossy fibers, prompting us to characterize and exploit this novel pharmacogenetic tool. P2X2 receptors are cell-surface ATP-gated cation channels that can be activated by synthetic ATP congeners (e.g., ATPγS). P2X2 receptors enter presynaptic terminals and axons, where their activation increases neurotransmitter release (Khakh and North, 2012). In light of this, we dubbed the mice with mossy fiber expression as "*SPRAE*" mice, an acronym for *S*elective *P*2X *R*eceptor *A*xoterminal *E*xcitation mice. As reported below, their activation triggered neurotransmitter release from mossy fibers, "spraying" the s.l. region with glutamate.

We found remarkably specific P2X2-YC expression within mossy fibers of *SPRAE* mice (Figure 4A), but not in WT mice (Figures S3D and S3E; n = 5). Striking expression was observed in the mossy fiber pathway, particularly within the terminal regions located in the s.l. (Figures S3G–S3I). We also evaluated the basic properties of granule cells from *SPRAE* mice in comparison to WT littermates and found no obvious differences (Figures S4A and S4B; n = 15–31). However, despite the absence of detectable P2X2-YC immunostaining within granule cell bodies, we did detect small somatic P2X2-YC-mediated currents in *SPRAE* mice (Figures S4C and S4D; n = 15–23; Figures S4E and S4F; n = 5 and 7). Overall, *SPRAE* mice display P2X2-YC expression in the mossy fibers, a feature we exploited to drive neurotransmitter release.

SPRAE Mice Permit Selective Glutamate Release from the Mossy Fiber Pathway

Mossy fiber boutons form synapses with CA3 pyramidal neurons via thorny excrescence spines in the s.l. (Amaral and Lavenex, 2007; Spruston and McBain, 2007) (Figure 4A). By monitoring glutamate mediated miniature (i.e., spontaneous) excitatory postsynaptic currents (mEPSCs) onto CA3 pyramidal neurons (in 0.5 μM TTX), we found that application of drug to activate P2X2-YC channels (ATPγS; 100 μM) dramatically increased their frequency. Similar responses were never observed in WT mice (Figure 4B). The large frequency increase made it difficult to measure all mEPSCs individually (Figure 4C), prompting us to measure charge transfer (nC). We measured charge transfer (nC) in 2 s bins during 30 min recordings before, during and after drug applications for *SPRAE* and WT mice (Figure 4D), revealing that ATPγS robustly triggered the release of glutamate onto pyramidal neurons from *SPRAE* mice but had no effect in WT mice (Figure 4D; n = 11 and 8). In seven out of eleven cells in the presence of TTX (0.5 μM) and Cd^{2+} (100 μM; Figure S4G; n = 11), all mEPSCs could be measured individually (in four cells they could not), revealing that ATPγS increased mEPSC frequency but not amplitude (Figures 4E–4G). In this experiment, the combination of TTX and Cd^{2+} was used to block action potential and voltage-gated Ca^{2+} channel dependent release.

In order to determine if mossy fiber filopodial terminals onto interneurons also express P2X2-YC in *SPRAE* mice, we repeated experiments shown in Figure 4 during recordings from s.l. interneurons. We found that ATPγS reliably increased glutamate release onto all interneurons examined in the *SPRAE* mice (Figure S5; n = 5 and 9). We also evaluated if activation of P2X2-YC in *SPRAE* mice released glutamate onto areas approximating the size of s.l. astrocytes by using 50 μm diameter glutamate biosensor electrodes and found that it did (Figure S6). Thus, *SPRAE* mice are a robust pharmacogenetic tool to selectively evoke glutamate release from hippocampal mossy fibers.

Astrocytes Display Prolonged Ca^{2+} Signals when Release from Mossy Fibers Is Increased

The combination of our findings with GCaMPs and *SPRAE* mice (Figures 1–4) presented an opportunity to directly determine if s.l. astrocytes (Figures 5A and 5B) display Ca^{2+} signals when neurotransmitter release from mossy fibers is elevated. We microinjected AAV2/5 for GCaMP3 into WT and *SPRAE* mice and monitored Ca^{2+} signals in s.l. astrocytes before, during, and after ATPγS applications to increase mossy fiber neurotransmitter release (Figures 5C and 5D). During control periods in both WT and *SPRAE* mice, we detected equivalent Ca^{2+} signals (Figures 5E and 5F), and as expected for WT mice (Figure 4), ATPγS produced no effect (Figures 5C and 5E; n = 9 cells). If astrocytes respond to quantal-like glutamate release, we would expect to observe more or prolonged Ca^{2+} signals in *SPRAE* mice during ATPγS applications. We found that ATPγS did not significantly increase astrocyte Ca^{2+} signal frequency or

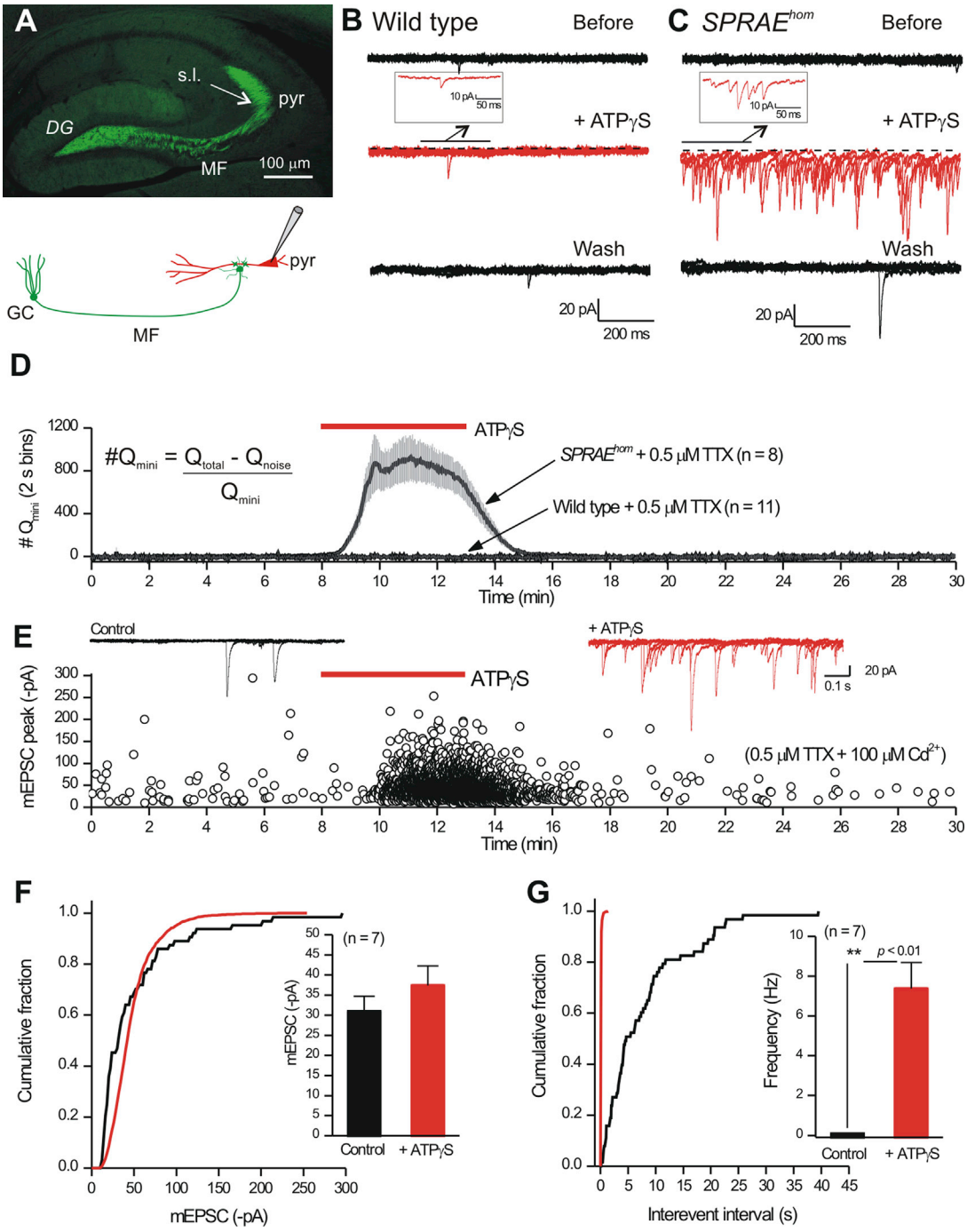

Figure 4. Activation of P2X2-YC Channels in the Mossy Fiber Pathway of *SPRAE* Mice Increases Glutamate Release onto CA3 Pyramidal Neurons

(A) P2X2-YC expression (green), from anti-GFP primary antibody and Alexa 488-conjugated secondary antibody, in the mossy fiber (MF) pathway. DG indicates the dentate gyrus, GC indicates granule cells, and pyr indicates the pyramidal cell layer.

(B) Five 1 s traces superimposed showing mEPSCs recorded from a CA3 pyramidal neuron from a WT mouse before, during, and after 100 μM ATPγS application.

(C) As in (B), but for recordings from *SPRAE*^{hom} mice.

(D) Quantification of experiments such as those shown in (B) and (C). The y axis plots the approximate number of quanta in 2 s bins. (Q_{mini} was measured from mEPSCs before the application of ATPγS, Q_{noise} was measured from silent periods, and Q_{total} was measured in 2 s bins.)

(E–G) (E) Traces and graphs show an exemplar neuron, showing an increase in frequency in the presence of ATPγS, but no increase in amplitude. Measuring all mEPSCs in 7/11 cells showed no increase in mEPSC amplitude ([F]; paired t test, $p < 0.05$), whereas frequency was increased ([G]; paired t test, $p < 0.01$). Experiments for CA3 interneurons are reported in Figure S5. Average data are shown as mean ±SEM.

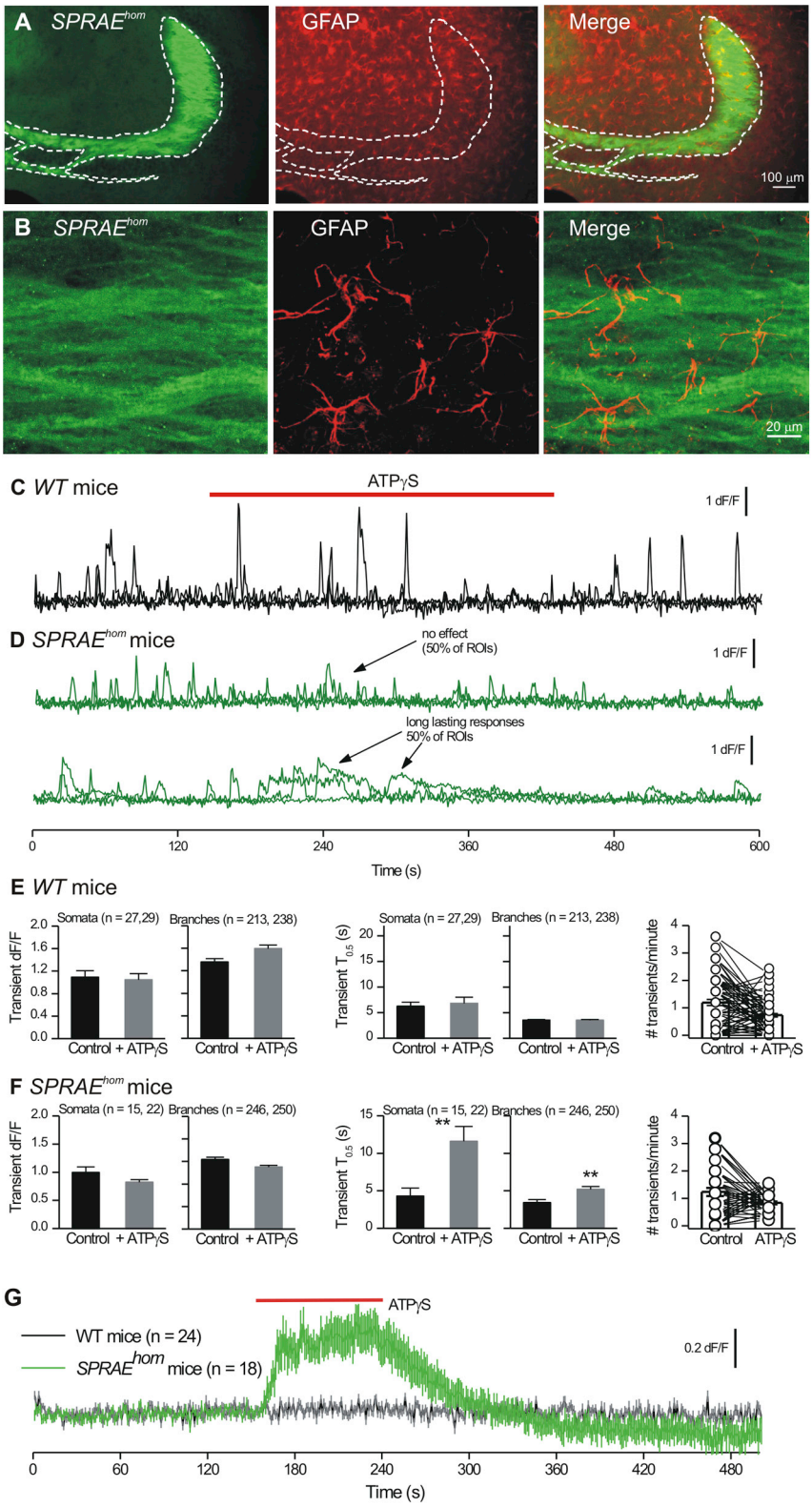

Figure 5. Stratum Lucidum Region Astrocyte Ca^{2+} Responses during Glutamate Release from Mossy Fibers in *SPRAE*^{hom} Mice

(A and B) (A) IHC for P2X2-YC in the mossy fibers (green) along with staining for astrocytes using GFAP (red); higher-magnification views shown in (B).

(C) Three representative traces superimposed for ROIs from astrocyte branches from a WT mouse before, during, and after 100 μM ATPγS applications for astrocytes located in the s.l.

(D) As in (C), but for astrocytes imaged from *SPRAE*^{hom} mice.

(E) Properties of astrocyte Ca^{2+} signals before and during ATPγS applications in WT mice.

(F) Properties of astrocyte Ca^{2+} signals before and during ATPγS applications in *SPRAE* mice. There was no significant difference in the duration of the spontaneous Ca^{2+} transients in *WT* and *SPRAE* mice before ATPγS. For somata, in *WT* mice their $T_{0.5}$ was 6.2 ± 0.9 s and in *SPRAE* mice the $T_{0.5}$ was 4.3 ± 1.1 s (n = 27 and 15; p = 0.16 with an unpaired t test). For branches, in *WT* mice their $T_{0.5}$ was 3.5 ± 0.2 s and in *SPRAE* mice the $T_{0.5}$ was 3.4 ± 0.4 s (n = 213 and 246; p = 0.83 with an unpaired t test).

(G) S.l. region astrocyte cell surface glutamate imaging with iGluSnFR in WT and *SPRAE*^{hom} mice. Average data are shown as mean ±SEM.

amplitude (Figures 5D and 5F; n = 10). However, ATPγS resulted in prolonged Ca^{2+} signals in ~50% of ROIs (Figure 5D), and this effect was statistically significant across all ROIs for *SPRAE* mice (Figure 5F; $p < 0.01$). The prolonged ATPγS-evoked events in *SPRAE* mice were significantly reduced in frequency in slices treated with CPA (Figure S7A; n = 7), implying store-mediated Ca^{2+} release. Given that ATPγS in *SPRAE* mice reliably elevates quantal-like glutamate release onto two neuronal targets of mossy fibers and broadly into the neuropil, this result provides evidence that high rates of glutamate release from mossy fiber terminals resulted in prolonged store-mediated astrocyte Ca^{2+} signals, which lasted up to 13 s (Figure 5F). This could happen because astrocytes respond to ambient levels of transmitter or to more frequent quantal-like events that result in the appearance of prolonged signals. In future work, these possibilities may be fruitfully explored with kinetic modeling when all the necessary parameters are known (Rusakov et al., 2011).

Astrocyte Cell Surface Glutamate Imaging with iGluSnFR in *SPRAE* Mice

Increasing neurotransmitter release from mossy fiber terminals caused prolonged Ca^{2+} signals in astrocyte somata and branches (Figure 5). To explore this, we used a genetically encoded glutamate sensor (Marvin et al., 2013) called iGluSnFR, expressed within

astrocytes. The glutamate affinity of iGluSnFR at ~5 μM (Figures S8A–S8C; n = 9) is in the range of the EC_{50} values for mGluRs, and therefore, it is a good indicator of whether or not mGluRs would be activated by the concentration of glutamate that reaches the astrocyte membrane. We made several observations with iGluSnFR. First, it was robustly expressed on the surface of astrocytes in the s.l. (Figure S8D). Second, we did not detect spontaneous iGluSnFR fluorescence increases in astrocytes from WT or *SPRAE* mice (Figures S8E–S8G; n = 24, 18), extending data in Figure 3. Third, in every astrocyte examined in *SPRAE* mice, we measured robust increases in iGluSnFR fluorescence over astrocyte territories in response to ATPγS applications (Figure 5G; Figures S8E–S8G; n = 18). Similar responses were never observed in WT mice (Figure 5G; Figures S8E–S8G; n = 24). These data provide direct evidence that micromolar glutamate is released from the mossy fibers onto astrocytes. Glutamate release is expected to be pulsatile from the mossy fibers themselves, but is it ambient or pulsatile in relation to much larger astrocyte territories that are distanced from release sites? Our data with biosensor electrodes show that glutamate levels are elevated within large areas of neuropil equivalent to whole astrocytes in *SPRAE* mice during ATPγS applications (Figure S6). In accord, our modeling of the kinetics of iGluSnFR also indicate that the baseline increase shown in Figure 9C represents an ambient increase in glutamate (Supplementary Note 1).

Astrocytes Display Ca^{2+} Signaling during Electrical Field Stimulation

To explore neurotransmitter mechanisms, we used local electrical field stimulation (EFS) with a glass microelectrode to evoke APs in the mossy fibers while imaging s.l. astrocytes. We found that single stimuli failed to evoke GCaMP3-observed Ca^{2+} signals in astrocyte branches or somata (Figures 6A–6C; n = 9–24) and that two stimuli were the minimum required to observe significant Ca^{2+} signals (Figures 6A and 6B; n = 9–24). Robust responses were seen for eight stimuli, and the relationship between stimulus number and somatic Ca^{2+} signals leveled out at 15 stimuli (Figure 6C; n = 9–24). By analyzing data for somata and branches separately, we found that the largest Ca^{2+} signals were seen for somata and that the relationship between EFS and branch Ca^{2+} signals was approximately linear (Figure 6C; n = 9–24). This linearity was due to an EFS-dependent increase in the occurrence of Ca^{2+} signals, which we measured as success rate (in % in Figures 6A and 6B). To determine if one stimulus did in fact release glutamate onto astrocyte branches, we performed parallel experiments with iGluSnFR. We found that the relationship between astrocyte iGluSnFR signals and EFS was different to that observed for Ca^{2+} signals measured with GCaMP3 (Figures 6D and 6E; n = 6). First, one stimulus was sufficient to evoke iGluSnFR signals, but not Ca^{2+} signals, which required at least two stimuli (*a* in Figure 6E). Second, the relationship between stimulus number and Ca^{2+} signals was approximately linear (*b* in Figure 6E). Third, during brief trains when astrocytes responded reliably to local EFS with iGluSnFR and Ca^{2+} signals, they did so quite globally, covering large areas of the astrocyte territory (e.g., eight stimuli; Figures 6F–6H).

We also performed a series of experiments to compare astrocyte Ca^{2+} responses to 1 and 15 EFS (Figure 7). Thus, we found that astrocytes from IP3R2 KO mice expressing GCaMP3 failed to respond to 1 or 15 EFS (Figures 7A and 7E; n = 9). Moreover, even with GCaMP6f we failed to detect astrocyte responses to 1 EFS, whereas 15 EFS worked reliably (Figures 7C and 7E; n = 9). We next used membrane-targeted Lck-GCaMP3 to explore the possibility that cytosolic GCaMP3 may have missed signals in near-membrane regions of processes. We found no evidence for any Lck-GCaMP3-detectable Ca^{2+} signals as a result of one EFS (Figures 7D and 7E; n = 11). Interestingly, using Lck-GCaMP3, we found that astrocyte reliability to 15 EFS was significantly reduced from 100% with GCaMP3 (Figures 6A and 6B) to 27% with Lck-GCaMP3 (Figure 7D) (n = 3 of 11 cells; $p < 0.01$ using unpaired Fisher's exact test). These data are consistent with those reported earlier (Table S1) and indicate that the majority of the spontaneous and EFS-evoked Ca^{2+} signals in s.l. astrocytes are mediated by intracellular stores. Thus overall, a variety of approaches (Figures 6 and 7) show that astrocyte branches "see" glutamate released following one EFS but that they do not detectably respond with an elevation of Ca^{2+} until bursts of stimuli are used. The s.l. astrocyte Ca^{2+} response to a single stimulus is undetectable with the full range of the methods that we employed or it does not exist.

Astrocyte Ca^{2+} Signaling during Action Potential Bursts Is Due to Glutamate and GABA

Having established that bursts of 8 and 15 stimuli evoke robust astrocyte GCaMP3-observed Ca^{2+} signals, we next explored the underlying neurotransmitter mechanisms by focusing on the branches (i.e., the sites of interaction with mossy fiber terminals). We used a two-pulse protocol, whereby 8 or 15 stimuli were applied twice to the mossy fibers, 8 min apart. This gave reproducible responses (Figures 8A and 8E; n = 6), and interpulse application of TTX (0.5 μM) abolished the second response (Figures 8B and 8E; n = 6). Because mossy fibers release glutamate onto astrocytes (Figures 6D and 6G) and because mature astrocytes express mGluR2/3 receptors (Sun et al., 2013), we began by applying the mGluR2/3 antagonist LY341495 (10 μM) and found that it significantly reduced EFS-evoked Ca^{2+} responses in astrocyte branches (Figures 8C and 8E; n = 7). However, even in the presence of LY341495, a residual EFS-evoked response persisted and was larger than that in the presence of TTX ($p < 0.05$ using Dunnett's ANOVA). This prompted us to explore a role for mGluR5 receptors: we found that a combination of LY341495 (10 μM) and MPEP (50 μM) did not reduce the responses any more than LY341495 alone (Figure 8E; n = 7). Taken together, these data suggest that glutamate release from mossy fibers evokes Ca^{2+} signals in astrocyte branches; ~50% are controlled via mGluR2/3 (Sun et al., 2013), with mGluR5 having a negligible contribution.

A variety of approaches show that mossy fibers also contain the molecular machinery to release GABA (Caiati, 2013; Gutiérrez, 2005; Walker et al., 2002), and ATP is thought to be released from nerve terminals in many CNS areas. In light of these facts, we evaluated if the residual response in the presence of LY341495 (Figures 8C and 8E) was mediated by P2Y or $GABA_B$ receptors that are known to elevate astrocyte Ca^{2+} signals in other areas of the hippocampus. We found that application of the P2Y1 antagonist MRS2179 (30 μM) was without effect

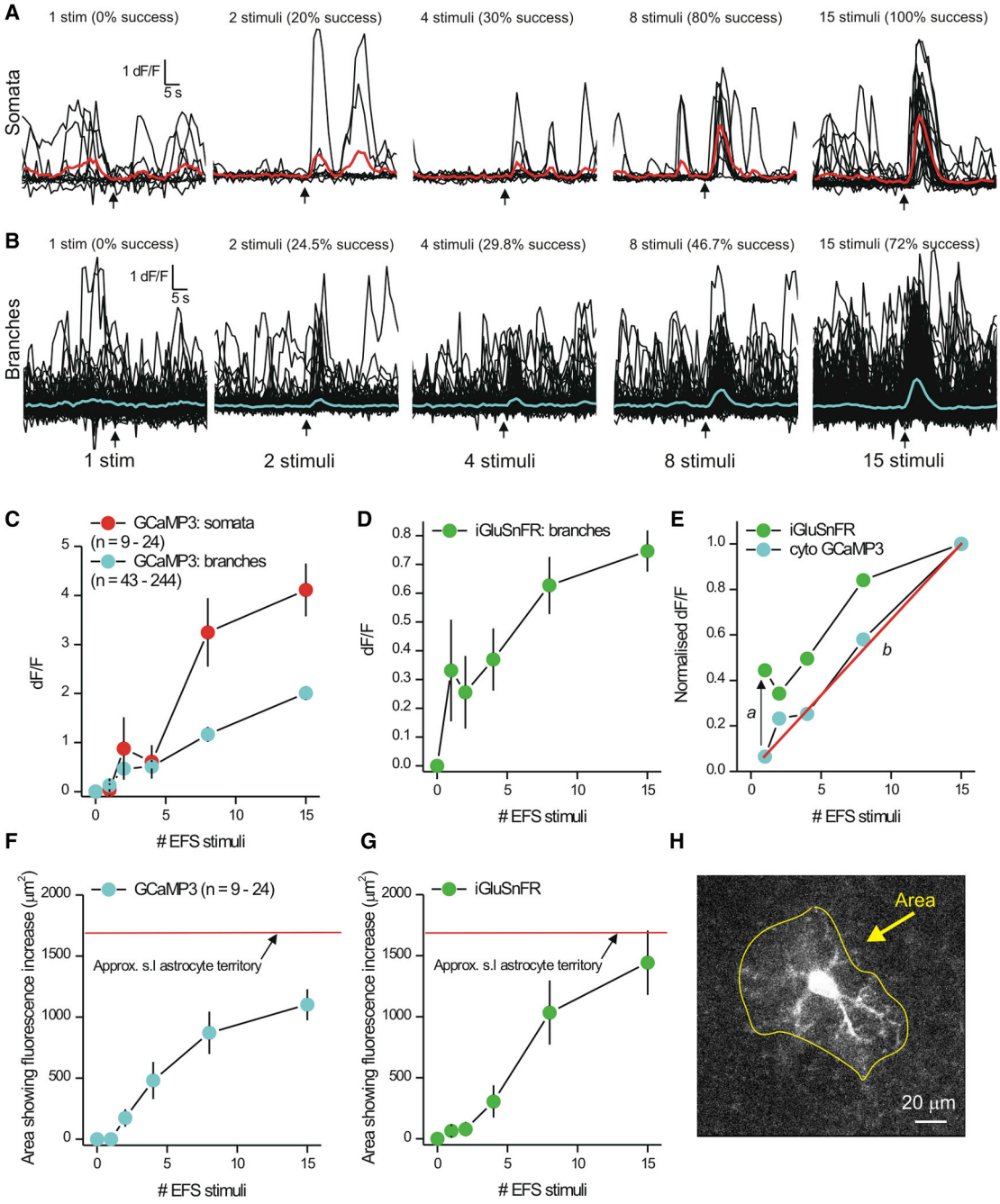

Figure 6. EFS Evokes Ca^{2+} Signaling in Astrocytes during Bursts of Stimuli

(A) GCaMP3 traces from astrocyte somata located in the s.l. region during local EFS of the mossy fiber pathway. The red traces are averages of the individual black traces. Signals were seen only for greater than two stimuli. The numbers above each set of traces indicate the success rate for each stimulus.

(B) As in (A), but for traces from branch ROIs; blue is an average of the individual black traces.

(C) Summary graph from experiments such as those shown in (A) and (B).

(D) The graph shows the increase in cell surface iGluSnFR fluorescence as a function of the number of local stimuli delivered to the mossy fiber terminals with EFS (n = 7–12).

(E) Plots the branchlet signals for Ca^{2+} and iGluSnFR: note the two plots do not overlap. In this plot, *a* indicates a threshold shift and *b* indicates that the relationship between Ca^{2+} signals in astrocyte branches and the number of stimuli was approximately linear.

(F) Plots the area of the astrocyte Ca^{2+} signals as a function of EFS stimuli and in relation to the territory of an s.l. astrocyte (Figure 1C).

(G) As in (F), but for iGluSnFR signals.

(H) Image of an s.l. astrocyte expressing GCaMP3 taken at the peak of 15 stimuli, showing Ca^{2+} elevation in most of its territory.

Average data are shown as mean ±SEM.

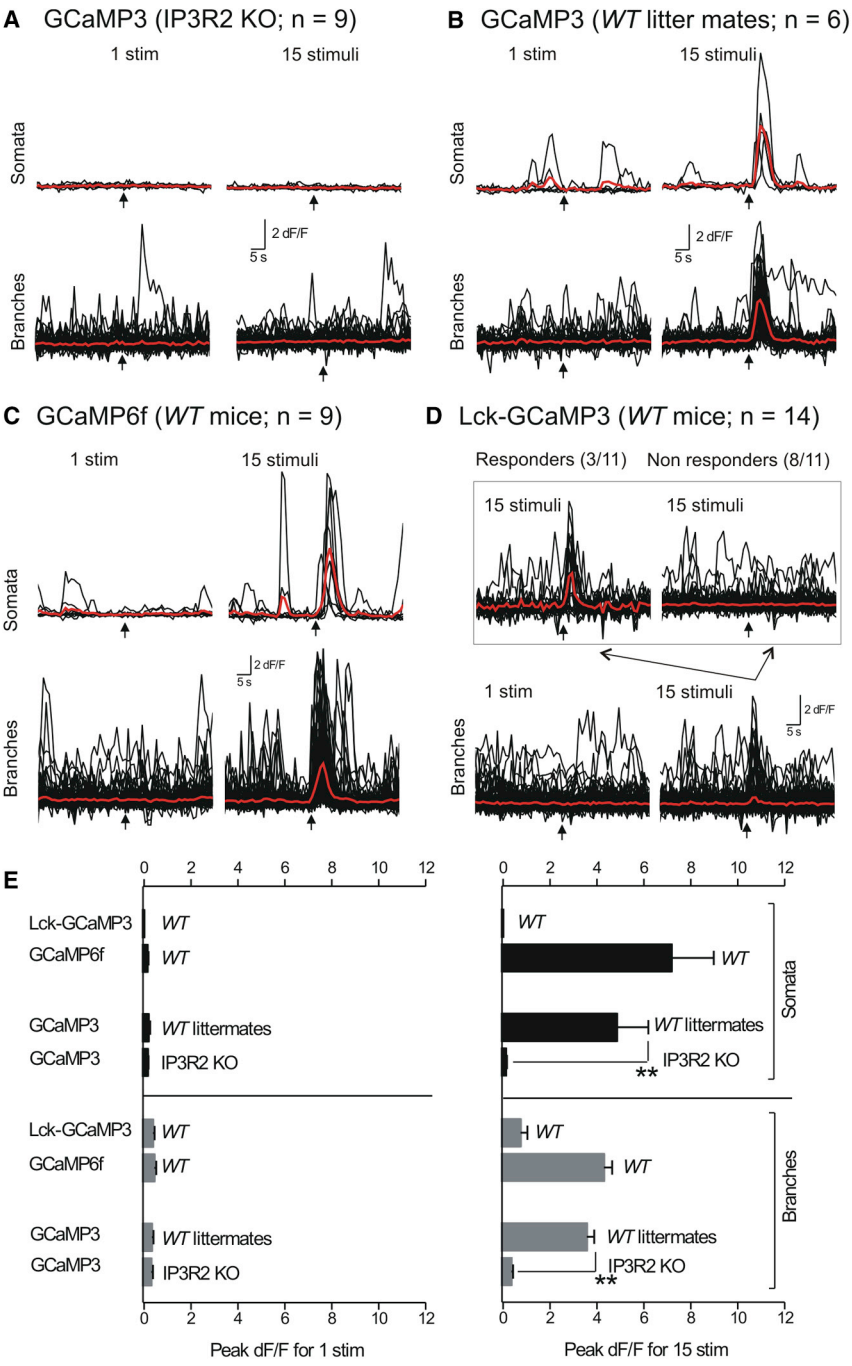

Figure 7. Evaluations of Astrocyte Responses to 1 and 15 Stimuli in IP3R2 KO Mice and with Various GECIs

(A–D) Ca^{2+} imaging traces for somata and branches before, during, and after EFS with 1 or 15 stimuli under the various conditions indicated. In the case of IP3R2 KO mice, comparative measurements were made with WT littermates (B).

(E) Bar graphs summarize average data from the experiments shown in (A)–(D). Average data are shown as mean ±SEM.

(Figure 8E; n = 7). However, we found that application of the $GABA_B$ receptor antagonist CGP52432 (10 μM) together with LY341495 reduced the EFS-evoked responses to levels below those observed with LY341495 alone (Figures 8D and 8E; n = 7). This was more clearly seen from ANOVA tests; in the presence of CGP52432 and LY341495, the EFS-evoked response was not statistically different to that in the presence of TTX ($p > 0.05$, Dunnett's ANOVA). Overall, these data indicate that astrocytes respond to glutamate and GABA release from mossy fiber terminals via mGluR2/3 and $GABA_B$ receptors, revealing a hitherto unknown potential physiological role for mossy fiber GABA release within this circuit. Consistent with this result, mGluR2/3 and $GABA_B$ receptor agonists elevated Ca^{2+} levels in s.l. astrocytes branches (in TTX), whereas an agonist of mGluR5 receptors did not (Figures 8F and 8G). Finally, in the *SPRAE* mice, a combination of CGP52432 and LY341495 also significantly reduced the number, peak amplitude, and duration of prolonged Ca^{2+} signals triggered by ATPγS applications (Figure S7B; n = 6).

Astrocyte Ca^{2+} Signaling in the Mossy Fiber Pathway Is Gated by Glutamate Clearance

Hippocampal astrocytes express high levels of GLT-1 and lower levels of GLAST glutamate transporters (Regan et al., 2007; Rothstein et al., 1996). In order to explore roles for glutamate clearance we applied the specific GLT-1/GLAST blocker TFB-TBOA (Huang et al., 2004) (300 nM) and found that it significantly increased EFS-evoked Ca^{2+} signals and duration in astrocyte branches (Figure 9A). These data provide further evidence that EFS-evoked astrocyte Ca^{2+} signals are mediated by glutamate (Figure 8) acting via mGluR2/3 receptors in astrocyte branches that appear not to be saturated. To further explore astrocyte engagement in the mossy fiber circuit, and its relation to glutamate uptake (Huang et al., 2004), we applied TBOA and monitored spontaneous Ca^{2+} signals in astrocyte branches, as well as astrocyte cell-surface glutamate signals with iGluSnFR (Figure 9). To our surprise, in the case of Ca^{2+} signals, we found that TBOA significantly increased their duration and frequency (Figures 9B and 9D–9F). TBOA also significantly increased the baseline iGluSnFR fluorescence of astrocytes, implying increased glutamate in the neuropil (Figures 9C and 9G; Supplemental Information), and it caused the appearance of brief pulsatile glutamate transients that could be easily observed with iGluSnFR (Figures 9C and 9G–9I). Given

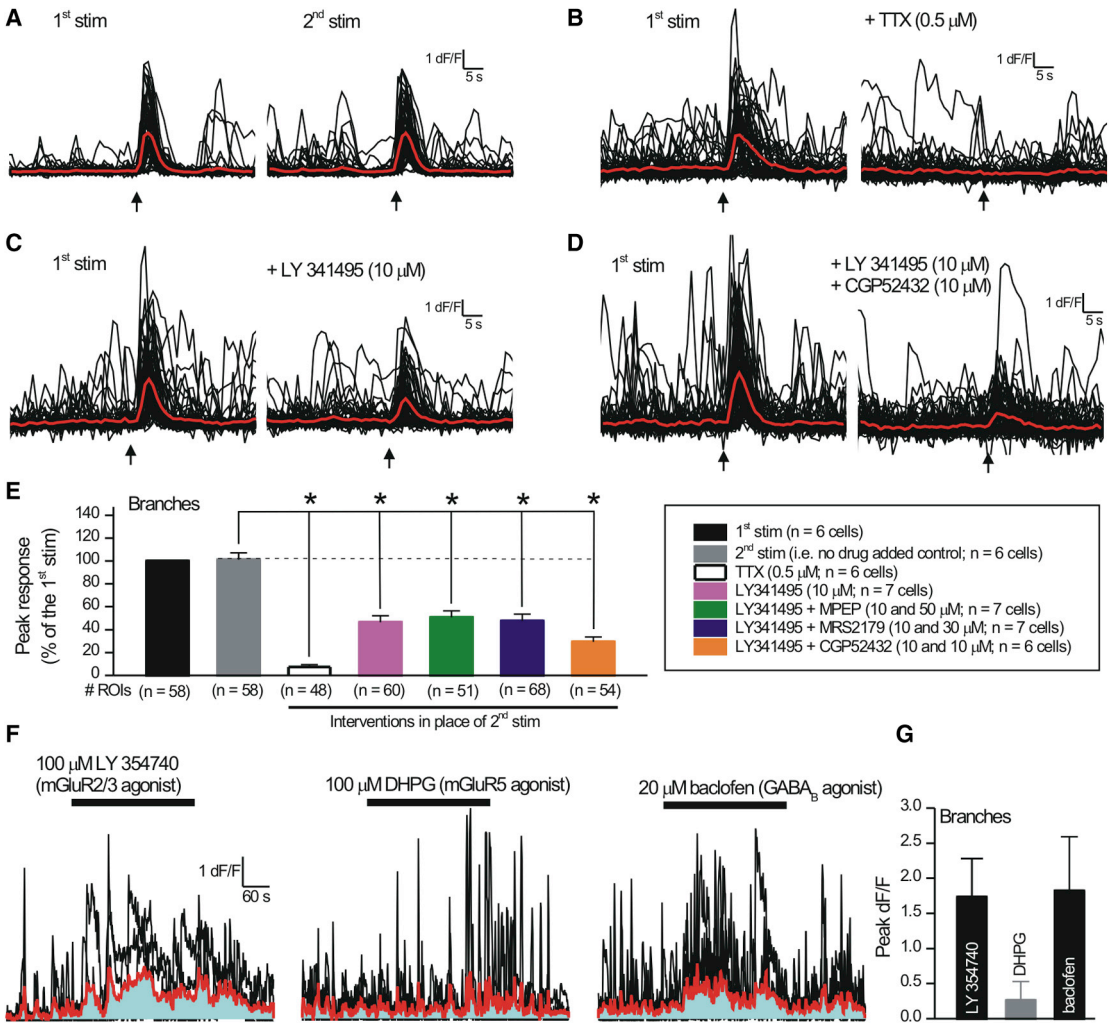

Figure 8. Electrical Field Stimulation Evokes Ca^{2+} Signals in Astrocytes that Are Mediated by Glutamate and GABA

(A) Traces show the protocol: two local EFS stimuli were delivered to the mossy fiber terminals 8 min apart.

(B) Application of TTX before the second EFS stimulation abolished the astrocyte Ca^{2+} signals.

(C) As in (B), but for applications of the mGluR2/3 receptor antagonist LY341495.

(D) As in (B), but for applications of the mGluR2/3 and $GABA_B$ receptor antagonists together (LY341495 and CGP52432).

(E) Summary bar graph for astrocyte branches from experiments such as those shown in (A)–(D), and for additional evaluations as indicated. The differences were analyzed using a Dunnett's ANOVA test, whereby all the treatments were compared to the control 2nd stimulation response.

(F) Representative traces (black) and average data (red) for agonist evoked Ca^{2+} signals in astrocyte branches. The area under the curve is shown in blue.

(G) Summary data for experiments such as those in (F).

Average data are shown as mean ±SEM.

that glutamate release does not normally contribute to spontaneous astrocyte Ca^{2+} or iGluSnFR signals (Figures 3 and 5), these data in the presence of TBOA provide compelling evidence that astrocyte engagement within the mossy fiber pathway is tightly gated by glutamate transporters.

We next used electron microscopy to explore proximity between astrocyte branches and mossy fiber synapses. We compared proximity between astrocytes and postsynaptic densities in the s.l. and at classical synaptic spines in the s.r. We observed that the relationship between postsynaptic densities and astrocyte branches was different for these two regions of the hippocampus. For the s.l. region, astrocyte branchlets surrounded the body of the large mossy fiber terminals and were peripherally located in relation to those for s.r. synapses (Figures 8J and 8K). We found that the shortest distance between a PSD and the nearest branchlet was twice as long for the s.l. as compared to the s.r. (Figure 9L; $n = 10$, $p < 0.05$). In the simplest interpretation that is also supported by our physiological measurements (Figures 2–9), astrocyte branchlets are located peripherally at mossy fiber synapses (Figures 9K and 9L) and are perhaps too distanced to detect transmitter release resulting from single stimuli. Our electron microscopy recalls past work (Rollenhagen and Lübke, 2006; Rollenhagen et al., 2007; Wilke et al., 2013).

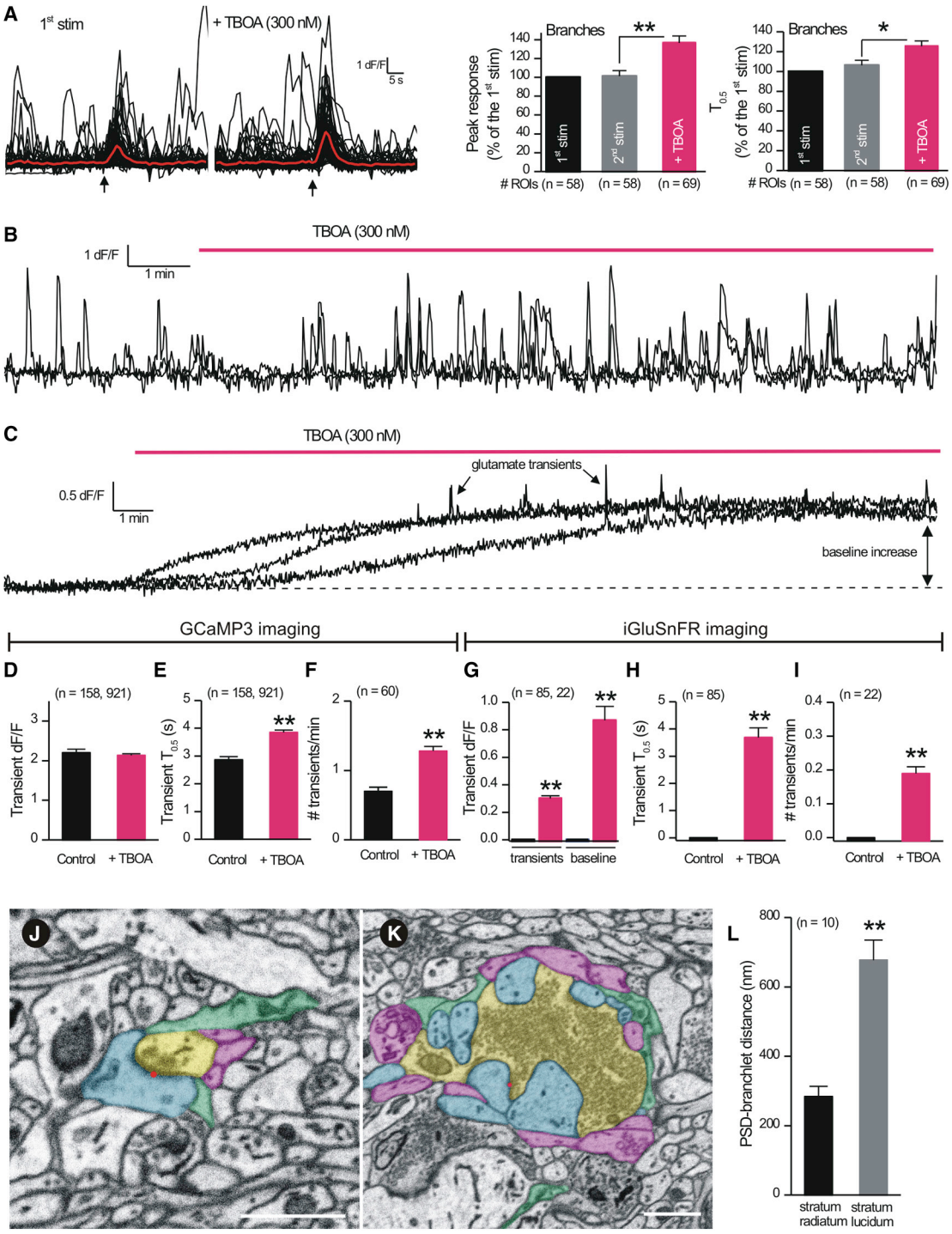

Figure 9. Glutamate Clearance Regulates EFS-Evoked and Spontaneous Ca^{2+} Signals in Astrocytes

(A) Traces for EFS-evoked astrocyte Ca^{2+} signals in branches before and during applications of TBOA (0.3 μM). The bar graphs to the right show average data, indicating that TBOA increased and prolonged EFS-evoked signals (Mann-Whitney test, $p < 0.05$).

(B) Traces for spontaneous Ca^{2+} signals in astrocyte branches before and during TBOA.

(C) As in (B), but for iGluSnFR glutamate signals. Note in the presence of TBOA the baseline increases and iGluSnFR transients are observed.

(D–F) Quantification of experiments such as those shown in (B). Statistical comparisons were made with paired t tests and significance declared at $p < 0.05$.

(G–I) Bar graphs show quantification of experiments such as those shown in (C). Statistical comparisons were made using the Wilcoxon signed-rank test and significance declared at $p < 0.05$.

(legend continued on next page)

DISCUSSION

We explored when and how astrocytes display Ca^{2+} signaling using novel optical and genetic tools in a mature model circuit with well-defined anatomy. We made several observations that may be portentous of circuits in general and that contribute to our understanding of astrocyte signaling in the mossy fiber pathway.

New Insights and Their Relation to Past Work

First, our study explores the details of astrocyte Ca^{2+} signaling in the mossy fiber pathway, which is a crucial limb of the hippocampal trisynaptic circuit. Our data form the basis to explore how astrocytes are engaged within, and contribute to, the function of the hippocampal circuit. As such, our work extends insights from the dentate gyrus (Di Castro et al., 2011) and s.r. regions (Panatier et al., 2011). In particular, the similarities and differences are important to note, because they may be physiologically relevant to each hippocampal region.

Second, s.l. region astrocyte Ca^{2+} signals can be studied using AAV2/5 viruses to express GCaMP3, which is an excellent GECI for studying astrocyte intracellular signals (Shigetomi et al., 2013a). Past experiments have reported Ca^{2+} signals in thick astrocyte branches a few micrometers from the soma in the dentate gyrus and s.r. (Di Castro et al., 2011; Panatier et al., 2011). However, by using GECIs, we observed a panorama of spontaneous and localized Ca^{2+} signals within almost entire astrocyte territories.

Third, astrocyte spontaneous Ca^{2+} signals were not driven by action potential firing or endogenous glutamate release, which is different to astrocytes in the dentate gyrus and s.r. (Di Castro et al., 2011; Panatier et al., 2011). We also did not detect spontaneous glutamate release onto astrocytes using iGluSnFR (Marvin et al., 2013), although we could readily measure neuronal-evoked glutamate release onto astrocytes. These observations are consistent with the fact that granule cells have strongly negative resting membrane potentials and low firing rates at rest (Ruiz and Kullmann, 2012). Moreover, these data also imply that glutamate release from s.l. astrocytes themselves is minimal.

Fourth, using transgenic *SPRAE* mice that allow the selective increase of neurotransmitter release from the mossy fibers, we found that astrocytes responded with prolonged Ca^{2+} signals that were significantly reduced by antagonists of mGluR2/3 and $GABA_B$ receptors (and increased by agonists to them).

Fifth, astrocytes responded to synaptic glutamate release during electrical stimulation of the mossy fibers, but only during bursts of stimuli. Under these circumstances (i.e., bursts), astrocyte Ca^{2+} signals covered large territory areas. This is different to astrocytes in the dentate gyrus and s.r. where astrocytes respond very locally to sparse action potentials and possibly even single vesicles (Di Castro et al., 2011; Panatier et al., 2011).

Sixth, astrocyte Ca^{2+} responses evoked by electrical stimulation were due to glutamate acting mainly via mGluR2/3 receptors and not via mGluR5 receptors, as in the s.r. of younger rats (Panatier et al., 2011). Our data are consistent with recent realizations that mGluR5 receptors are not expressed in adult astrocytes (Sun et al., 2013). Interestingly, a small component of the electrically evoked response was mediated by GABA acting at $GABA_B$ receptors. This is relevant in the context of the mossy fiber pathway, because GABA is released from the mossy fibers (Caiati, 2013; Walker et al., 2002) and astrocytes express Ca^{2+} mobilizing $GABA_B$ receptors (Kang et al., 1998).

Seventh, astrocyte Ca^{2+} signaling was tightly gated by glutamate clearance. Thus, when glutamate uptake was blocked, we observed enhanced spontaneous Ca^{2+} signals, enhanced iGluSnFR glutamate signals onto astrocytes, and elevated electrically evoked astrocyte responses. Our data do not simply show that glutamate transporters regulate spontaneous Ca^{2+} signals. Rather, they unexpectedly show that glutamate transporters gate the engagement of astrocytes and spontaneous Ca^{2+} signals. Glutamate transporters were not considered in past work (Di Castro et al., 2011; Panatier et al., 2011).

Eighth, by monitoring astrocyte Ca^{2+} signaling and glutamate signals during electrical stimulation of the mossy fibers, we found that astrocytes sense glutamate reliably, even during a single stimulus to the mossy fibers, but translate this to Ca^{2+} signaling less efficiently. Moreover, when Ca^{2+} signaling is observed, it increases over entire territories.

Ninth, a study on the adult cortex showed that astrocyte Ca^{2+} responses to whisker stimulation were partly mediated by synaptic release of glutamate acting on astrocyte mGluR5 receptors (Wang et al., 2006), whereas a recent study concluded that glutamatergic signaling is insufficient to trigger astrocyte Ca^{2+} signaling (Sun et al., 2013). Our data extend these findings by showing that s.l. astrocytes respond to synaptic glutamate release during bursts of activity or during high amounts of quantal-like release in *SPRAE* mice (via mGluR2/3 and $GABA_B$ receptors). The use of GECIs may permit similar studies of other brain regions and prepare us for the possibility that astrocytes may have microcircuit specific properties, emphasizing the need for caution in generalizing from one brain region to another.

Tenth, and more broadly for evaluations of astrocytes throughout the brain, our studies provide a tool kit that is useful to explore physiological astrocyte responses in detail. As recently discussed (Li et al., 2013), these tools do not replace organic Ca^{2+} indicator dyes, but are demonstrably better for exploring astrocyte territories and branches.

Ca^{2+} Signal Properties and Kinetics

Using GCaMP3 imaging, we found evidence for numerous spontaneous Ca^{2+} signals throughout astrocytes. By pooling data across identical control conditions, our summary data show that Ca^{2+} signals in somata and branches display $T_{0.5}$ values of

(J and K) Images of the arrangement of cellular elements around boutons located in the s.r. (J) and s.l. (K). Postsynaptic spines (blue) form a larger, more complex synaptic complex with boutons (yellow) in the s.l. Red dots indicate location of a PSD. Astrocyte processes (green) are generally more distal from PSDs in s.l. than in s.r. Neighboring axons not forming boutons also surround synapse in both areas (purple). Scale bars = 1 micron.
(L) Graph summarizes the shortest distances from a PSD to an astrocyte branchlet for the stratum radiatum and s.l. Average data are shown as mean ±SEM.

4.4 ± 0.16 and 3.1 ± 0.04 s, respectively, when imaged by GCaMP3 (329 and 3,757 events from 65 cells). Ca^{2+} signals also lasted seconds (~3 s) when detected by GCaMP6f, and we found no evidence for faster Ca^{2+} signals. Interestingly, we observed fewer signals with Lck-GCaMP3, implying that Ca^{2+} signals in s.l. astrocytes are mainly intracellular in origin. In accord, the signals were significantly reduced in mice that lacked IP3R2s. Thus, differences exist between s.l. and s.r. astrocytes (Shigetomi et al., 2013a, 2013b), likely reflecting the existence of astrocyte heterogeneity in different hippocampal regions. Irrespectively, all the spontaneous signals we observed in s.l. astrocytes were slow, revealing fundamental constraints on how quickly astrocytes can track to neuronal input in this pathway. Moreover, our data showed that a statistically insignificant number of astrocyte spontaneous Ca^{2+} signals were due to action potential firing or endogenous glutamate release, which is in accord with the known electrical properties of the mossy fiber pathway (Ruiz and Kullmann, 2012).

A recent proposal is that astrocytes respond to and regulate single synapses in the dentate gyrus and s.r. (Di Castro et al., 2011; Panatier et al., 2011). A key line of evidence was the finding that astrocytes displayed localized Ca^{2+} signals when quantal release probability was elevated using high-osmotic-strength sucrose (Di Castro et al., 2011), implying that astrocytes respond during quantal-like glutamate release. Cognizant of these findings and their implications for the function of microcircuits, we took advantage of *SPRAE* mice generated in our laboratory. Activation of P2X2-YC channels with drug increased mEPSCs onto all CA3 pyramidal neurons, all s.l. interneurons, broadly into the s.l. neuropil, and resulted in prolonged astrocyte Ca^{2+} signals in *SPRAE* mice. The glutamate released from mossy fibers readily reached astrocyte branches, because we could detect it using iGluSnFR where it increased the duration of Ca^{2+} signals. More generally, *SPRAE* mice may be useful in future work to explore outstanding questions in mossy fiber physiology (Ruiz and Kullmann, 2012).

Can the kinetics of the Ca^{2+} signals we measured with GCaMP3, GCaMP6f, and Lck-GCaMP3 be directly compared to the kinetics of signals measured with organic Ca^{2+} dyes in other parts of the hippocampus (Di Castro et al., 2011; Panatier et al., 2011)? Although the affinities of the indicators employed are similar, we still suggest caution in this regard, because it is well established that the same Ca^{2+} dynamics will be reported differently by different Ca^{2+} indicators depending on their concentration and affinity. Hence, kinetic modeling is needed to explore precisely how astrocyte Ca^{2+} signals appear as observables with distinct imaging approaches. As recently highlighted, the field of astrocyte biophysics lags behind similar studies of neurons by decades (Rusakov et al., 2011). From this perspective, our work lays the foundations for future experimental and modeling work.

Evoked Responses and Tight Gating of Astrocyte Engagement by Glutamate Transporters

Using EFS of mossy fibers, we found that s.l. region astrocytes responded to bursts of stimuli rather than a single stimulus when we used GCaMP3 or GCaMP6f. This is reminiscent of past work (D'Ascenzo et al., 2007; Gordon et al., 2009). S.l. astrocytes responded unreliably to all examined forms of EFS when imaged using Lck-GCaMP3, which supports the view that the Ca^{2+} signals have an intracellular origin. Our use of iGluSnFR directly showed that single stimuli to the mossy fibers release sufficient amounts of glutamate to reach astrocyte branches, implying that s.l. astrocytes are ineffective postsynaptic responders to sparse action potentials. Moreover, with bursts of stimuli, astrocytes appear to respond proportionately to the number of stimuli applied to the mossy fibers, with increases in Ca^{2+} that covered entire territories and large areas of neuropil. This may be a powerful entrainment mechanism to control release of substances from astrocytes. On the basis of these data, we conclude that the physiological role of astrocyte Ca^{2+} signaling in the s.l. region is to respond to bursts of activity and functionally segregate large areas of neuropil over a time course of seconds. We suggest that the most likely consequence for neuronal circuit activity is increased local blood flow (Attwell et al., 2010); homeostatic regulation via release of slow neuromodulators such as adenosine, D-serine, and ions; and perhaps release of synaptogenic factors broadly in the vicinity of synapses that need them. In future work, these possibilities need to be systematically explored when methods to selectivity block and precisely mimic physiological astrocyte Ca^{2+} signals have been developed.

The receptors on s.l. region astrocyte branches that respond to neurotransmitter release from mossy fibers appear to be mGluR2/3 and $GABA_B$ receptors. Although mGluR2/3 and $GABA_B$ are coupled to $G_{i/o}$ G-proteins, the $\beta\gamma$-subunits mediate Ca^{2+} release from intracellular stores by activating phospholipase C directly or by interaction with IP3 receptors (Zeng et al., 2003). Interestingly, a previous study employing mGluR2/3 receptor agonists to study cortical astrocytes using bulk loading of Ca^{2+} indicator dyes was not able to evaluate Ca^{2+} signals in branches (Sun et al., 2013). Using GCaMP3, we were able to monitor astrocyte branches directly in adult brain slices and show that mGluR2/3 receptors mediate neuron-astrocyte functional interactions on the time scale of seconds and on distance scales of whole astrocyte territories (~1,500 μm^2), implying astrocytes do not act as sensors of single synapses or sparse activity.

Finally, our data show that spontaneous and evoked astrocyte Ca^{2+} signaling is tightly gated by glutamate uptake via GLT-1 and GLAST glutamate transporters (Rothstein et al., 1996). Glutamate uptake may be expected to regulate astrocyte Ca^{2+} signals, but our data unexpectedly show that the function of glutamate transporters acts as a gate for spontaneous Ca^{2+} signals. Given that glutamate uptake is compromised in many brain disorders (Kanai et al., 2013), our data suggest that the contribution of glutamate-mediated astrocyte Ca^{2+} signaling for the function of neuronal circuits is likely to be particularly manifest during disease (Agulhon et al., 2012). This realization also suggests an explanation for why abolishing astrocyte intracellular-store-mediated Ca^{2+} signals was without any major consequence in healthy mice. If so, astrocyte roles need to be explored in disease models (Agulhon et al., 2012), and astrocytes may represent targets for therapeutic development to treat neurological and psychiatric disorders.

EXPERIMENTAL PROCEDURES

Molecular Biology and Adenovirus (AAV 2/5) Generation

Viruses were made as described (Shigetomi et al., 2013a). Our virus constructs have been deposited at Addgene in the Khakh lab repository (http://www.addgene.org/Baljit_Khakh). The AAVs are also available from the UPenn Vector Core (http://www.med.upenn.edu/gtp/vectorcore).

Surgery and In Vivo Microinjections of AAV 2/5

Postnatal day 56 to 63 (P56–P63) male and female C57BL/6N or *SPRAE* mice were used in all experiments in accordance with institutional guidelines. All surgical procedures were conducted under general anesthesia using continuous isoflurane (induction at 5%; maintenance at 1%–2.5% vol/vol). Following induction of anesthesia, the mice were fitted into a stereotaxic frame with their heads secured by blunt ear bars and their noses placed into an anesthesia and ventilation system (David Kopf Instruments, Tujunga). Mice were administered 0.05 ml of buprenorphine (Buprenex; 0.1 mg/ml) subcutaneously prior to surgery. The surgical incision site was then cleaned three times with 10% povidone iodine and 70% ethanol. Skin incisions were made, followed by craniotomies of 2–3 mm in diameter above the left parietal cortex using a small steel burr (Fine Science Tools) powered by a high-speed drill (K.1070, Foredom). Saline (0.9%) was applied onto the skull to reduce heating caused by drilling. Unilateral viral injections were carried out by using a stereotaxic apparatus (David Kopf Instruments) to guide the placement of beveled glass pipettes (1B100-4, World Precision Instruments) into the left hippocampus (2 mm posterior to bregma; 2 mm lateral to midline; 2.2 mm from the pial surface). Either 2 μl of AAV2/5 gfaABC$_1$D Lck-GCaMP3 (1.2×10^{13} gc/ml), 2 μl of AAV2/5 GfaABC$_1$D GluSnFr (4.2×10^{12} gc/ml), 1.5μl of AAV2/5 gfaABC$_1$D Lck-GFP (2.41×10^{13} gc/ml), 1.5 μl of AAV5 gfaABC$_1$D GCaMP6f (2.4×10^{13} gc/ml), or 1.5 μl of AAV2/5 gfaABC$_1$D GCaMP3 (1.5×10^{13} gc/ml) was injected by using a syringe pump (Pump11 PicoPlus Elite, Harvard Apparatus). Glass pipettes were left in place for at least 10 min. Surgical wounds were closed with single external 6-0 nylon sutures. Following surgery, animals were allowed to recover overnight in cages placed partially on a low-voltage heating pad. Buprenorphine was administered two times per day for up to 2 days after surgery. In addition, trimethoprim/sulfamethoxazole (40 and 200 mg, respectively, per 500 ml water) was dispensed in the drinking water for 1 week. Mice were sacrificed 14–20 days postsurgery for imaging (typically 14–16 days).

Mice

The generation of *SPRAE* mice is described in detail in the Supplementary Information. IP3R2 KO mice were obtained from Dr. Ju Chen at UCSD and maintained as a heterozygous line (Li et al., 2005). Homozygotes and WT littermates were used for experiments when they reached age P56–P80.

Preparation of Brain Slices and Ca^{2+} Imaging

Coronal slices of hippocampus (300 μm) were cut in solution comprising the following (in mM): 87 NaCl, 25 $NaHCO_3$, 2.5 KCl, 1.25 NaH_2PO_4, 25 D-glucose, 75 sucrose, 7 $MgCl_2$, and 0.5 $CaCl_2$ saturated with 95% O_2 and 5% CO_2 (pH 7.4). Slices were incubated at ~34°C for 30 min and subsequently stored at room temperature in artificial cerebrospinal fluid (aCSF) comprising the following (in mM): 126 NaCl, 2.5 KCl, 1.3 $MgCl_2$, 10 D-glucose, 2.4 $CaCl_2$, 1.24 NaH_2PO_4, and 26 $NaHCO_3$ saturated with 95% O_2 and 5% CO_2 (pH 7.4). All other slice procedures were exactly as described (Shigetomi et al., 2008). All our imaging was performed using commercially available confocal microscopes. In brief, cells were imaged using an Olympus Fluoview 300 confocal microscope with a 40× water immersion objective lens with a numerical aperture of 0.8 or with the Olympus Fluoview 1000 confocal microscope using the same lens. We used the 488 nm line of an Argon laser, with the intensity adjusted to 5%–10% of the maximum output, which was 16.9 mW in the case of the Fluoview 300 and 10 mW in the case of the Fluoview 1000. The emitted light pathway consisted of an emission high pass filter (>510 nm) before the photomultiplier tube. Framescans were recorded at 1 frame/s and linescans at 200 Hz. For electrical stimulation a glass pipette (1B150-4, WPI) with a tip resistance of 3–5 MΩ was filled with a solution comprising the following (in mM): 130 NaCl, 30 HEPES, and 5 Glucose, adjusted to pH 7.3 with NaOH and connected to a Grass S88 Stimulator via the Stimulus Isolator A360 (WPI). The tip of the electrode was placed in the mossy fiber pathway at 30–80 μm (usually 40–50 μm) distance from the astrocyte. Individual pulses were 1 ms in duration, and stimuli were delivered at 40 μA with 1, 2, 4, 8, or 15 pulses/s at a rate of 15 Hz. All imaging experiments with *SPRAE* mice were performed in the presence of TTX (0.5 μM) as well as MRS2179 (30 μM) and DPCPX (10 μM) to block P2Y1 and adenosine A1 receptors, respectively, on astrocytes (Figure S4H).

Electron Microscopy

Serial block-face scanning electron microscope (SBEM) volumes of mouse CA3 s.l. and CA1 stratum radiatum were used for analyzing astrocyte-PSD distances. The original data set was collected as part of a recent study (Wilke et al., 2013) but was reanalyzed here to specifically measure the distances. Briefly, a mouse (P14) was perfused with 2.5% glutaraldehyde/2.0% paraformaldehyde in cacodylate buffer, and the tissue was sectioned and stained for SBEM imaging as previously described (Deerinck et al., 2010). The IMOD software package was used to perform analysis of astrocyte branchlet-to-PSD distances (Kremer et al., 1996). For both s.l. and stratum radiatum, PSDs were initially marked with a point at their center. All astrocytic branchlets in the surrounding neuropil were manually segmented to generate 3D surfaces. The IMOD tool mtk was used to measure the distance from the PSD to each astrocyte surface.

SUPPLEMENTAL INFORMATION

Supplemental Information includes eight figures, two tables, four movies, and Supplemental Experimental Procedures and can be found with this article online at http://dx.doi.org/10.1016/j.neuron.2014.02.041.

AUTHOR CONTRIBUTIONS

Most of the experiments were done by M.D.H. (imaging) and B.S.K. (electrophysiology). The BAC mice were made by S.K. with guidance from X.-H.L. and X.W.Y. The electron microscopy work was done by T.S., E.A.B., and M.H.E. J.S.M. and L.L.L. shared unpublished reagents/data and did the modeling work. O.J-.W., T.J.O., X.T., and J.X. contributed to the experimental aspects (molecular biology, electrophysiology, and imaging). B.S.K. wrote the paper. All authors contributed to the final version.

ACKNOWLEDGMENTS

Most of this work was supported by NIH grant NS060677 and partly by NIH grants MH099559 and MH104069 (BSK). O.J-.W. was partly supported by T32 NS007101. X.W.Y. was supported by the NIH grants NS049501 and NS074312. TS., M.H.E., and E.A.B. were supported by an award from NIH/NIGMS P41GM103412, which funds the National Center for Microscopy and Imaging Research. Special thanks to A. Ghosh and S. Wilke for sharing SBEM data sets that were reanalyzed here. Thanks to R. Serrano for help analyzing line scan data. Thanks to M.V. Sofroniew for sharing equipment. Thanks also to R. Huckstepp for help with setting up the glutamate biosensors. Thanks to R. Srinivasan for help with GCaMP6f virus generation. Many thanks to Ju Chen (UCSD) for sharing IP3R2 KO mice. Thanks to current and former members of the Khakh lab for their input and help.

Accepted: February 13, 2014
Published: April 16, 2014

REFERENCES

Agulhon, C., Petravicz, J., McMullen, A.B., Sweger, E.J., Minton, S.K., Taves, S.R., Casper, K.B., Fiacco, T.A., and McCarthy, K.D. (2008). What is the role of astrocyte calcium in neurophysiology? Neuron *59*, 932–946.

Agulhon, C., Fiacco, T.A., and McCarthy, K.D. (2010). Hippocampal short- and long-term plasticity are not modulated by astrocyte Ca2+ signaling. Science *327*, 1250–1254.

Agulhon, C., Sun, M.Y., Murphy, T., Myers, T., Lauderdale, K., and Fiacco, T.A. (2012). Calcium signaling and gliotransmission in normal vs. reactive astrocytes. Front. Pharmacol *3*, http://dx.doi.org/10.3389/fphar.2012.00139.

Amaral, D., and Lavenex, P. (2007). Hippocampal neuroanatomy. In The Hippocampus Book, Chapter 3, P. Andersen, R. Morris, D. Amaral, T. Bliss, and J. O'Keefe, eds. (Oxford: Oxford University Press), pp. 37–114.

Attwell, D., Buchan, A.M., Charpak, S., Lauritzen, M., Macvicar, B.A., and Newman, E.A. (2010). Glial and neuronal control of brain blood flow. Nature *468*, 232–243.

Caiati, M.D. (2013). Is GABA co-released with glutamate from hippocampal mossy fiber terminals? J. Neurosci. *33*, 1755–1756.

Chen, T.W., Wardill, T.J., Sun, Y., Pulver, S.R., Renninger, S.L., Baohan, A., Schreiter, E.R., Kerr, R.A., Orger, M.B., Jayaraman, V., et al. (2013). Ultrasensitive fluorescent proteins for imaging neuronal activity. Nature *499*, 295–300.

D'Ascenzo, M., Fellin, T., Terunuma, M., Revilla-Sanchez, R., Meaney, D.F., Auberson, Y.P., Moss, S.J., and Haydon, P.G. (2007). mGluR5 stimulates gliotransmission in the nucleus accumbens. Proc. Natl. Acad. Sci. USA *104*, 1995–2000.

Deerinck, T.J., Bushong, E.A., Lev-Ram, V., Shu, X., Tsien, R.Y., and Ellisman, M.H. (2010). Enhancing serial block-face scanning electron microscopy to enable high resolution 3-D nanohistology of cells and tissues. Microsc. Microanal. *16*, 1138–1139, http://dx.doi.org/10.1017/S1431927610055170.

Di Castro, M.A., Chuquet, J., Liaudet, N., Bhaukaurally, K., Santello, M., Bouvier, D., Tiret, P., and Volterra, A. (2011). Local Ca2+ detection and modulation of synaptic release by astrocytes. Nat. Neurosci. *14*, 1276–1284.

Fiacco, T.A., Agulhon, C., Taves, S.R., Petravicz, J., Casper, K.B., Dong, X., Chen, J., and McCarthy, K.D. (2007). Selective stimulation of astrocyte calcium in situ does not affect neuronal excitatory synaptic activity. Neuron *54*, 611–626.

Gordon, G.R., Iremonger, K.J., Kantevari, S., Ellis-Davies, G.C., MacVicar, B.A., and Bains, J.S. (2009). Astrocyte-mediated distributed plasticity at hypothalamic glutamate synapses. Neuron *64*, 391–403.

Gutiérrez, R. (2005). The dual glutamatergic-GABAergic phenotype of hippocampal granule cells. Trends Neurosci. *28*, 297–303.

Huang, Y.H., Sinha, S.R., Tanaka, K., Rothstein, J.D., and Bergles, D.E. (2004). Astrocyte glutamate transporters regulate metabotropic glutamate receptor-mediated excitation of hippocampal interneurons. J. Neurosci. *24*, 4551–4559.

Kanai, Y., Clémençon, B., Simonin, A., Leuenberger, M., Lochner, M., Weisstanner, M., and Hediger, M.A. (2013). The SLC1 high-affinity glutamate and neutral amino acid transporter family. Mol. Aspects Med. *34*, 108–120.

Kang, J., Jiang, L., Goldman, S.A., and Nedergaard, M. (1998). Astrocyte-mediated potentiation of inhibitory synaptic transmission. Nat. Neurosci. *1*, 683–692.

Khakh, B.S., and North, R.A. (2012). Neuromodulation by extracellular ATP and P2X receptors in the CNS. Neuron *76*, 51–69.

Kremer, J.R., Mastronarde, D.N., and McIntosh, J.R. (1996). Computer visualization of three-dimensional image data using IMOD. J. Struct. Biol. *116*, 71–76.

Kuffler, S.W. (1967). Neuroglial cells: physiological properties and a potassium mediated effect of neuronal activity on the glial membrane potential. Proc. R. Soc. Lond. B Biol. Sci. *168*, 1–21.

Li, X., Zima, A.V., Sheikh, F., Blatter, L.A., and Chen, J. (2005). Endothelin-1-induced arrhythmogenic Ca2+ signaling is abolished in atrial myocytes of inositol-1,4,5-trisphosphate(IP3)-receptor type 2-deficient mice. Circ. Res. *96*, 1274–1281.

Li, D., Agulhon, C., Schmidt, E., Oheim, M., and Ropert, N. (2013). New tools for investigating astrocyte-to-neuron communication. Front. Cell Neurosci *7*, 193.

Marvin, J.S., Borghuis, B.G., Tian, L., Cichon, J., Harnett, M.T., Akerboom, J., Gordus, A., Renninger, S.L., Chen, T.W., Bargmann, C.I., et al. (2013). An optimized fluorescent probe for visualizing glutamate neurotransmission. Nat. Methods *10*, 162–170.

Panatier, A., Vallée, J., Haber, M., Murai, K.K., Lacaille, J.C., and Robitaille, R. (2011). Astrocytes are endogenous regulators of basal transmission at central synapses. Cell *146*, 785–798.

Petravicz, J., Fiacco, T.A., and McCarthy, K.D. (2008). Loss of IP3 receptor-dependent Ca2+ increases in hippocampal astrocytes does not affect baseline CA1 pyramidal neuron synaptic activity. J. Neurosci. *28*, 4967–4973.

Reeves, A.M., Shigetomi, E., and Khakh, B.S. (2011). Bulk loading of calcium indicator dyes to study astrocyte physiology: key limitations and improvements using morphological maps. J. Neurosci. *31*, 9353–9358.

Regan, M.R., Huang, Y.H., Kim, Y.S., Dykes-Hoberg, M.I., Jin, L., Watkins, A.M., Bergles, D.E., and Rothstein, J.D. (2007). Variations in promoter activity reveal a differential expression and physiology of glutamate transporters by glia in the developing and mature CNS. J. Neurosci. *27*, 6607–6619.

Richler, E., Chaumont, S., Shigetomi, E., Sagasti, A., and Khakh, B.S. (2008). Tracking transmitter-gated P2X cation channel activation in vitro and in vivo. Nat. Methods *5*, 87–93.

Rollenhagen, A., and Lübke, J.H. (2006). The morphology of excitatory central synapses: from structure to function. Cell Tissue Res. *326*, 221–237.

Rollenhagen, A., Sätzler, K., Rodríguez, E.P., Jonas, P., Frotscher, M., and Lübke, J.H. (2007). Structural determinants of transmission at large hippocampal mossy fiber synapses. J. Neurosci. *27*, 10434–10444.

Rothstein, J.D., Dykes-Hoberg, M., Pardo, C.A., Bristol, L.A., Jin, L., Kuncl, R.W., Kanai, Y., Hediger, M.A., Wang, Y., Schielke, J.P., and Welty, D.F. (1996). Knockout of glutamate transporters reveals a major role for astroglial transport in excitotoxicity and clearance of glutamate. Neuron *16*, 675–686.

Ruiz, A.J., and Kullmann, D.M. (2012). Ionotropic receptors at hippocampal mossy fibers: roles in axonal excitability, synaptic transmission, and plasticity. Front. Neural Circuits *6*, 112. Published online Jan 9, 2013. http://dx.doi.org/10.3389/fncir.2012.00112.

Rusakov, D.A., Zheng, K., and Henneberger, C. (2011). Astrocytes as regulators of synaptic function: a quest for the Ca2+ master key. Neuroscientist *17*, 513–523.

Shigetomi, E., Bowser, D.N., Sofroniew, M.V., and Khakh, B.S. (2008). Two forms of astrocyte calcium excitability have distinct effects on NMDA receptor-mediated slow inward currents in pyramidal neurons. J. Neurosci. *28*, 6659–6663.

Shigetomi, E., Kracun, S., Sofroniew, M.V., and Khakh, B.S. (2010). A genetically targeted optical sensor to monitor calcium signals in astrocyte processes. Nat. Neurosci. *13*, 759–766.

Shigetomi, E., Tong, X., Kwan, K.Y., Corey, D.P., and Khakh, B.S. (2011). TRPA1 channels regulate astrocyte resting calcium and inhibitory synapse efficacy through GAT-3. Nat. Neurosci. *15*, 70–80.

Shigetomi, E., Bushong, E.A., Haustein, M.D., Tong, X., Jackson-Weaver, O., Kracun, S., Xu, J., Sofroniew, M.V., Ellisman, M.H., and Khakh, B.S. (2013a). Imaging calcium microdomains within entire astrocyte territories and endfeet with GCaMPs expressed using adeno-associated viruses. J. Gen. Physiol. *141*, 633–647.

Shigetomi, E., Jackson-Weaver, O., Huckstepp, R.T., O'Dell, T.J., and Khakh, B.S. (2013b). TRPA1 channels are regulators of astrocyte basal calcium levels and long-term potentiation via constitutive D-serine release. J. Neurosci. *33*, 10143–10153.

Spruston, N., and McBain, C. (2007). Structural and functional properties of hippocampal neurons. In The Hippocampus Book, P. Andersen, R. Morris, D. Amaral, T. Bliss, and J. O'Keefe, eds. (Oxford: Oxford University Press).

Sun, W., McConnell, E., Pare, J.F., Xu, Q., Chen, M., Peng, W., Lovatt, D., Han, X., Smith, Y., and Nedergaard, M. (2013). Glutamate-dependent neuroglial calcium signaling differs between young and adult brain. Science *339*, 197–200.

Tian, L., Hires, S.A., Mao, T., Huber, D., Chiappe, M.E., Chalasani, S.H., Petreanu, L., Akerboom, J., McKinney, S.A., Schreiter, E.R., et al. (2009). Imaging neural activity in worms, flies and mice with improved GCaMP calcium indicators. Nat. Methods *6*, 875–881.

Tian, L., Akerboom, J., Schreiter, E.R., and Looger, L.L. (2012). Neural activity imaging with genetically encoded calcium indicators. Prog. Brain Res. *196*, 79–94.

Tong, X., Shigetomi, E., Looger, L.L., and Khakh, B.S. (2013). Genetically encoded calcium indicators and astrocyte calcium microdomains. Neuroscientist *19*, 274–291.

Walker, M.C., Ruiz, A., and Kullmann, D.M. (2002). Do mossy fibers release GABA? Epilepsia *43* (*Suppl 5*), 196–202.

Wang, X., Lou, N., Xu, Q., Tian, G.F., Peng, W.G., Han, X., Kang, J., Takano, T., and Nedergaard, M. (2006). Astrocytic Ca2+ signaling evoked by sensory stimulation in vivo. Nat. Neurosci. *9*, 816–823.

Wilke, S.A., Antonios, J.K., Bushong, E.A., Badkoobehi, A., Malek, E., Hwang, M., Terada, M., Ellisman, M.H., and Ghosh, A. (2013). Deconstructing complexity: serial block-face electron microscopic analysis of the hippocampal mossy fiber synapse. J. Neurosci. *33*, 507–522.

Zariwala, H.A., Borghuis, B.G., Hoogland, T.M., Madisen, L., Tian, L., De Zeeuw, C.I., Zeng, H., Looger, L.L., Svoboda, K., and Chen, T.W. (2012). A Cre-dependent GCaMP3 reporter mouse for neuronal imaging in vivo. J. Neurosci. *32*, 3131–3141.

Zeng, W., Mak, D.O., Li, Q., Shin, D.M., Foskett, J.K., and Muallem, S. (2003). A new mode of Ca2+ signaling by G protein-coupled receptors: gating of IP3 receptor Ca2+ release channels by Gbetagamma. Curr. Biol. *13*, 872–876.